

Telescope Optics and Weak Lensing: PSF Patterns due to Low Order Aberrations

Mike Jarvis¹, Paul Schechter², Bhuvnesh Jain¹

¹*Department of Physics and Astronomy, University of Pennsylvania, Philadelphia, PA 19104*

²*Department of Physics, MIT, Cambridge, MA 02138*

ABSTRACT

In weak lensing investigations, galaxy shapes are corrected for the convolution by the point spread function (PSF) using stellar images. In this paper we use physical models of the telescope optics to understand the spatial variation of the PSF in the image plane. We introduce a set of parameters to model the key aberrations, which include defocus, focal plane tilt, primary and off-axis astigmatism, and coma. We also include the effects of guiding and seeing. We test our model with data from the Blanco 4 meter telescope in Cerro Tololo, Chile. We find that the physical model describes a substantial part of the PSF size and anisotropy over the field of view (over 90 percent of it, based on a chi-squared metric). We identify the primary contributors to the PSF patterns and study their covariances and principal components. We also identify correlations with the effect of gravity on the telescope. Finally, we discuss the improvements in PSF estimation that may be achieved by combining the physical model in this study with the purely empirical approach of Jarvis and Jain (2004).

Subject headings: cosmology:gravitational lensing, telescope optics

1. Introduction

The weak gravitational lensing of background galaxies by foreground galaxies has proven itself a powerful technique for studying the largest structures in the universe (e.g. Schneider 2006). But on the largest angular scales, the coherent distortions of galaxy images due to lensing can be as small as one part in one thousand. The reliable measurement of such small effects requires a thorough understanding of instrumental and observational effects that might masquerade as weak lensing.

No telescope produces perfectly circular images. The extent to which those images deviate from perfect circularity depends upon the design of the telescope and the degree to which the telescope maintains its alignment. Gravity, thermal effects, mechanical oscillations and operator error can all cause images to be elliptical.

The practioners of weak lensing calibrate their instruments by measuring the shapes of stars, which are effectively delta functions before passing through the atmosphere and telescope. The typical high galactic latitude field has relatively few stars, but by averaging over many such fields or by using fields with many more stars (e.g. Hoekstra 2004), one can improve the PSF estimation.

Unfortunately most of the phenomena that cause elliptical PSF images are time variable. Typical exposures and time averages correct only for that part of the instrumental PSF that is time invariant.

With too few stars in a single exposure to produce a precise map of the PSF, a model is needed to track such temporal variations. Such models might be calculated from first principles (“theoretical” models), purely empirical, or some combination of the two.

An example of the empirical approach would be the efforts of Jarvis & Jain (2004) who looked at the principal components of the PSF shapes for a thousand images taken with the BTC and Mosaic cameras on the Victor Blanco telescope. For every exposure one can then calculate the projection of its PSF pattern onto a limited subset of those principal components and correct accordingly. Jarvis & Jain (2004) also offer physical interpretations for the largest of their principal components. Their first principal component seems to be telescope focus. The second appears to reflect tracking errors.

There are several benefits if the physics dominating one or more of these principal components can be identified. Foremost, one might then address the underlying cause and remove the source of the pattern. Second, there is no guarantee that a single principal component has a single physical cause (and no guarantee that physical effects produce orthogonal principal components). If one models known causes of the PSF shape directly, it opens the possibility that physical causes can be identified for the remaining principal components. Finally a physical model may be more accurate than a principal component, which is derived from noisy and incomplete data.

There are three main sources of PSF ellipticity produced by a telescope (apart from those that are a direct consequence of the telescope design): guiding errors, misaligned optics, and deformations of the primary mirror. These sources can vary with time, hence their effect varies from one exposure to another. The first and third of these however have the same effect across the entire field, producing the same shape in all star and galaxy images in a given exposure. This makes it easy to correct for them.

Misaligned optics, however, produce aberration patterns that vary across the field. These patterns take particularly simple forms when expanded as polynomials in wavefront error (e.g. Mahajan 1991; Schroeder 1999). The lowest order terms relevant for weak lensing are called focus, astigmatism and coma. As described in §2 below, nine numbers suffice to characterize the focus, astigmatism, and coma patterns that result from first order telescope misalignments. The problem of modeling the PSF due to optical aberrations may therefore not be as daunting as it might first seem.

In §2 we review low order telescope aberrations. In §3 we describe the patterns produced by telescope misalignments. In §4 we discuss the aberrations produced by deformations of the primary mirror. In §5 we examine the PSF patterns from a few hundred exposures taken with the Blanco telescope. We interpret them in the context of telescope misalignments and primary mirror deformations.

2. Review of Low Order Aberrations

Image aberrations are conveniently described using a power series expansion of the wavefront, with coordinates ρ and θ described on the telescope pupil (i.e. the plane of the primary mirror), where the dimensionless radial coordinate ρ is taken to be unity at the outer boundary of a circular pupil. Mahajan (1991) and Schroeder (1999) give, respectively, exhaustive treatments of aberration theory in general and telescope aberrations in particular. The two lowest order polynomials describe a change in phase of the wavefront and a tilt of the wavefront, neither of which is relevant for the present discussion. The next lowest terms in the expansion are called defocus, astigmatism, coma and spherical aberration, all of which are relevant to the present discussion.

One can look at the PSF either in the focal (image) plane or the wavefront projected onto the pupil. In physical optics they constitute a Fourier pair. For weak lensing, the image plane PSF is the primary quantity of interest, but telescope aberrations are more easily described in terms of their effect on the wavefront in the pupil plane. This is because, in the pupil plane, the effect of multiple aberrations add linearly in the wavefront, but have a more complex interaction in the image plane. That is the approach followed in this section. In §3 we will describe the variation of the aberrations in the image plane.

2.1. Defocus

The focus is adjusted by moving the focal plane along the optical axis (or by moving a mirror to create the same effect). However, we can project the effect of the defocus on the wavefront back to the primary mirror to describe it in pupil coordinates.

The resulting defocus, $\delta\lambda_{\text{defocus}}$, is given by

$$\delta\lambda_{\text{defocus}} = A_{\text{defocus}}\rho^2 \quad (1)$$

Assuming, as is the case for ground based telescopes, that the images are not diffraction limited, the effect of the wavefront on image quality is readily understood by considering the gradient of the wavefront, which is,

$$\nabla\delta\lambda_{\text{defocus}} = 2A_{\text{defocus}} (\rho \cos \theta \hat{x} + \rho \sin \theta \hat{y}) \quad (2)$$

The outer panels of Figure 1 shows the gradient of the wavefront for two images with equal and opposite amounts of defocus. It may be helpful to think of the defocus as arising from slope errors on the primary mirror. Dividing the pupil into small equal area segments, the point spread function (PSF) is then computed by plotting one point for each segment, with the angular deflection from perfect focus proportional to the gradient of the wavefront (the effective focal length being the constant of proportionality). For the two cases illustrated in the left and right panel of Figure 1, the resulting PSF is a boring, uniformly illuminated circular disk.

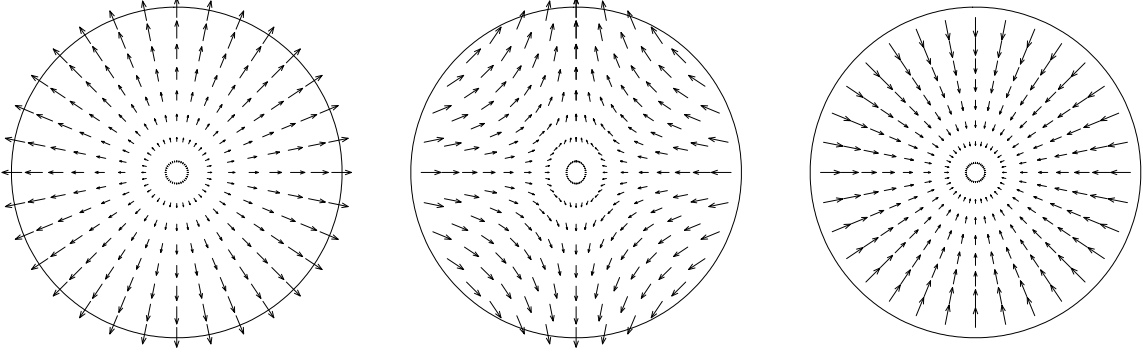


Fig. 1.— Wavefront slope errors projected onto a circular pupil. The left and right show slope errors for positive and negative defocus. The center shows slope errors for pure astigmatism. At every point in the three figures the slope errors have the same magnitude. But the slope vectors for astigmatism are reflected about the vertical (horizontal) axis with respect to the defocus vectors on the left (right). Combining the astigmatism vectors with the defocus vectors on the left (right) produces a PSF that is a straight vertical (horizontal) line.

2.2. Astigmatism

The primary cause of astigmatism is an overall warping of the primary mirror, but as we discuss below, there are other causes which lead to a variable astigmatism over the field of view.

There are two independent components to the astigmatism of a wavefront, $\delta\lambda_{\text{astig-c}}$, and $\delta\lambda_{\text{astig-s}}$, given by

$$\delta\lambda_{\text{astig-c}} = A_{\text{astig-c}}\rho^2 \cos 2\theta \quad (3)$$

$$\delta\lambda_{\text{astig-s}} = A_{\text{astig-s}}\rho^2 \sin 2\theta \quad (4)$$

The gradients of these two components are given by

$$\nabla\delta\lambda_{\text{astig-c}} = 2A_{\text{astig-c}} (\rho \cos \theta \hat{x} - \rho \sin \theta \hat{y}) \quad (5)$$

$$\nabla\delta\lambda_{\text{astig-s}} = 2A_{\text{astig-s}} (\rho \sin \theta \hat{x} + \rho \cos \theta \hat{y}) \quad (6)$$

Since both components are purely quadratic in wavefront, the sum of two purely astigmatic contributions to the wavefront is again purely astigmatic. One can always find a coordinate system in which the second component is zero, so in what follows we will use a single coefficient A_{astig} . The central panel of Figure 1 shows the gradient of the wavefront for the first of the two astigmatism components. (A gradient plot for the second component would be rotated by 45 deg.)

It is instructive to compare the lengths and orientations of the gradient vectors in the three panels of Figure 1. At every point in each of the three panels the vectors are the same length. In the first and last panels (the two defocused wavefronts) the vectors point in opposite directions. In the central panel (the

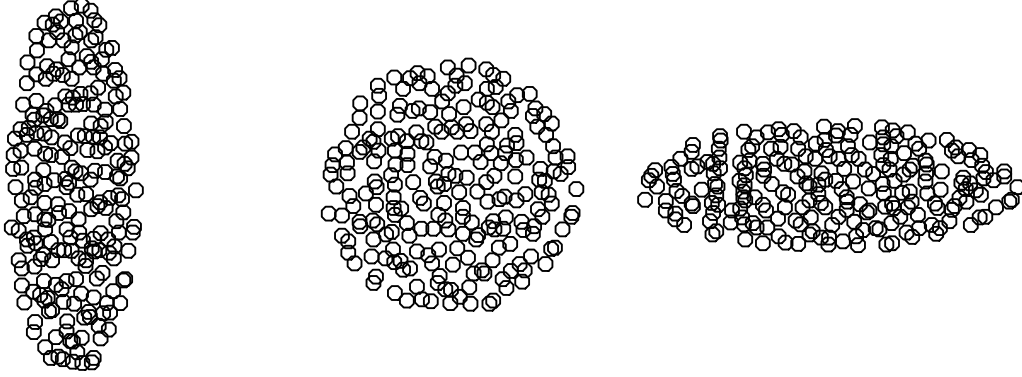


Fig. 2.— The center shows the point spread function obtained from the purely astigmatic slope errors shown in the center of Figure 1. The left (right) shows the PSF obtained from adding one half the defocus shown on the left (right) of Figure 1 to the astigmatism shown in the center of that figure. The spot displacements have been randomized by roughly 10%. A combination of astigmatism *and* defocus is needed to produce elliptical images.

astigmatic wavefront) one of the Cartesian components is the same as in the adjacent panel while the other has the opposite sign. This has important consequences for the ellipticity of images and for weak lensing.

The gradient vectors in the central panel in Figure 1 may be used to calculate the PSF for the astigmatic wavefront. This is done simply by collecting the heads of all the vectors at the center so that the arrows of the vectors represent the PSF. The result is shown in the central panel of Figure 2. Some readers may be surprised to see that the PSF of an astigmatic image is circular. This is a direct consequence of the fact that the wavefront gradient vectors are the same as for a defocused image, except for a switch in sign of one of the two coordinates.

But astigmatic images are never perfectly in focus. If we add defocus with plus or minus half the amplitude of the astigmatism, we get the flattened PSFs seen in the left and right panels of Figure 2. Non-round PSF images are the result of astigmatism *and* defocus. A straightforward calculation shows that the difference in second moments of such an image is proportional to the *product* of the astigmatism and the defocus. If we added and subtracted defocus with the same amplitude as the astigmatism in Figure 2, the PSFs would be lines of finite length. Adding and subtracting still more defocus produces rounder images (but with the difference between the second moments nonetheless increasing).

Astigmatic images have the character that the rays are converging too quickly in one direction and too slowly in the orthogonal direction. On one side of focus they converge to a line. As one approaches focus they start to diverge while the rays in the orthogonal direction are still converging. On the other side of focus these rays then converge to a line, perpendicular to the first.

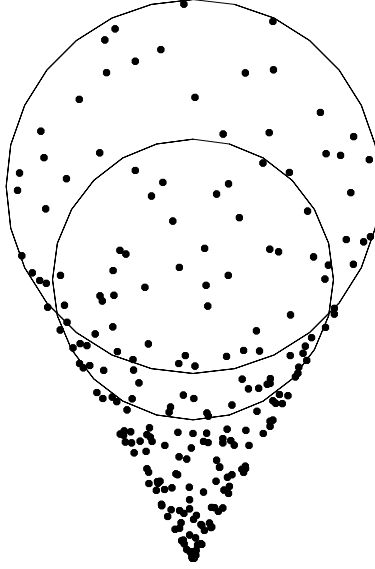


Fig. 3.— The point spread function produced by a purely comatic wavefront. The larger circle indicates the locus of spots produced by the outer edge of the pupil. The smaller circle indicates the locus of spots produced by points on the pupil 6/7th of the way to the edge.

2.3. Coma

Coma is famously associated with Newtonian telescopes, which use a parabola for the primary mirror. The center of the field of view focuses correctly, but as an image moves further from the optical axis, the parabola no longer focuses the light from different parts of the mirror onto the same point. Modern telescopes use corrector lenses to account for this effect.

As with astigmatism, there are two independent components to the coma of a wavefront, $\delta\lambda_{\text{coma-c}}$, and $\delta\lambda_{\text{coma-s}}$, given by

$$\delta\lambda_{\text{coma-c}} = A_{\text{coma-c}} (\rho^3 - \rho) \cos \theta \quad (7)$$

$$\delta\lambda_{\text{coma-s}} = A_{\text{coma-s}} (\rho^3 - \rho) \sin \theta \quad (8)$$

The gradients of these two components are given by

$$\nabla \delta\lambda_{\text{coma-c}} = A_{\text{coma-c}} ((2\rho^2 - 1 + \rho^2 \cos 2\theta) \hat{x} + \rho^2 \sin 2\theta \hat{y}) \quad (9)$$

$$\nabla \delta\lambda_{\text{coma-s}} = A_{\text{coma-s}} (\rho^2 \sin 2\theta \hat{x} + (2\rho^2 - 1 - \rho^2 \cos 2\theta) \hat{y}) \quad (10)$$

We note that the ρ term needs to be included so that the centroid in the image plane is zero. In general, coma does move the centroid of the PSF, but we care more about the shape than the position, so we choose this form to avoid a spurious contribution to the second moments from a non-zero centroid.

A comatic PSF is illustrated in Figure 3. The rays coming from the center of the pupil lie very close together. Those from the outer boundary of the pupil lie on a circle offset to one side of the more central rays.

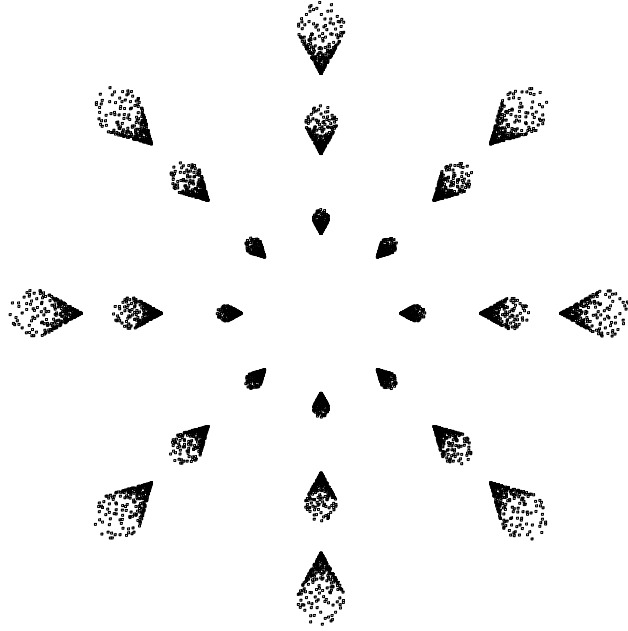


Fig. 4.— Off-axis comatic point spread functions produced at the prime focus of a parabolic mirror. The size of the PSF increases linearly with distance from the center of the field, and points outward.

A comatic PSF is completely specified by an amplitude and a direction. In this regard, the comatic PSF behaves like a vector. The sum of two different comatic wavefronts again gives a comatic wavefront. Moreover, the resulting PSF has an amplitude and direction given by the rules of vector addition. We can therefore treat the comatic PSF as a vector.

By contrast, the PSF of an astigmatic image cannot be treated as a vector. There is a twofold ambiguity in assigning a direction to an astigmatic PSF, hence the PSF that results from the addition of two astigmatic wavefronts cannot be obtained by simple vector addition of the two astigmatic point spread functions.

2.4. Spherical Aberration

The last aberration we consider is spherical aberration, which, as the name suggests, is associated with the primary mirror being more spherical than parabolic. Modern telescopes with multiple optical elements can reduce both this and coma at once to a large extent, but they can never completely eliminate both. Therefore, while we don't expect this to be something that varies from one exposure to the next, there may be a constant spherical aberration due to incomplete correction in the telescope design or errors in the positions of some of the optical elements.

The effect of spherical aberration is given by

$$\delta\lambda_{\text{spherical}} = A_{\text{sph}}\rho^4 \quad (11)$$

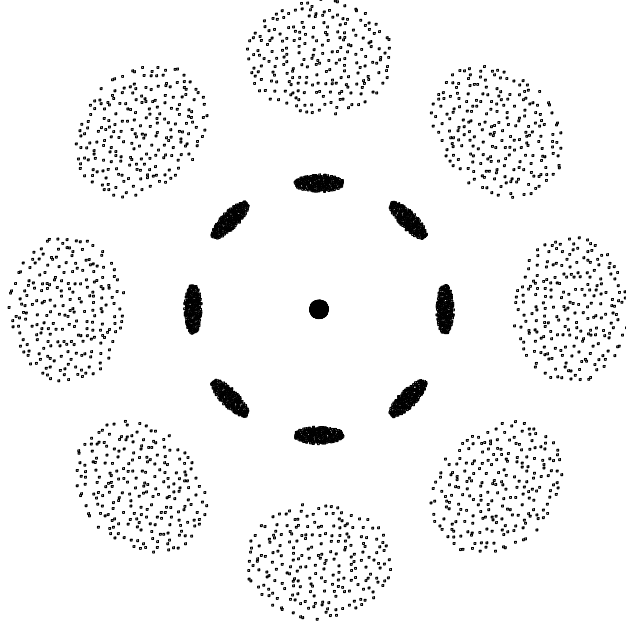


Fig. 5.— Off-axis astigmatic point spread functions produced at the prime focus of a parabolic mirror. In the absence of defocus the PSF would be circular and would increase quadratically with distance from the center of the field. A small amount of defocus, indicated by the spot at the center, has been added to highlight the potential for astigmatism to produce elliptical images.

$$\nabla \delta \lambda_{\text{sph}} = 4A_{\text{sph}} (\rho^3 \cos \theta \hat{x} + \rho^3 \sin \theta \hat{y}) \quad (12)$$

3. Miscalculated Off-Axis Aberrations

A paraboloidal mirror produces perfect images on-axis. But off-axis images suffer from coma, which increases linearly with distance from the axis, and astigmatism, which increases quadratically with distance from the axis. In this section we will consider the PSF resulting from these two aberrations and describe their variation in the image plane (in contrast to the pupil plane description of wavefront error in §2).

Weak lensing requires wide fields, and the telescopes used to study weak lensing have what are in effect “correctors” for off-axis coma and astigmatism. A prime focus telescope like the Blanco 4-meter at Cerro Tololo has a multi-element transmitting corrector close to the prime focus. A Ritchey-Chretien telescope (e.g. Schroeder 1999) like the ESO 2.2-meter on La Silla is corrected for off-axis coma by making the primary mirror slightly hyperbolic and balancing this with a hyperbolic secondary that is slightly different from what it would otherwise be in a straight Cassegrain configuration. A transmitting corrector close to the secondary focus (e.g. Bowen and Vaughn 1972) then corrects for astigmatism.

For our purposes it suffices to imagine a single corrector close to the focal plane. If all of the optical elements are aligned the telescope produces perfect images (or more likely very slightly imperfect images).



Fig. 6.— The point spread function caused by miscorrecting for off-axis astigmatism. The figures on the left and right are obtained by taking two copies of figure 5, shifting one vertically with respect to the other and then subtracting one from the other. A small amount of defocus has been added to the figure on the left and subtracted from the figure on the right. If one had a misaligned corrector, one would expect to see one pattern or the other as the focus varied. Since *all* correctors are misaligned, the question is only one of degree.

But if the corrector is displaced perpendicular to the optical axis, the wrong correction is applied to the images. The wavefront arriving at the detector is given by the difference between the correction needed and the correction applied.

No telescope is ever perfectly aligned. The most careful alignment process will still produce small but hopefully tolerable misalignments. More seriously, thermal stresses, variable gravitational forces and human error all lead to misalignments.

3.1. Off-Axis Coma

By virtue of its linear dependence, off-axis coma presents less of challenge for weak lensing than astigmatism. In Figure 4 we show the linear growth of off-axis coma with distance from the axis. The pattern may be represented by a vector field, directed outward from the axis. A coma corrector would produce a vector field directed inward. If the corrector is displaced perpendicular to the optical axis, the difference between the two vectors fields is everywhere a vector constant. Therefore two numbers suffice to describe the mis-correction of off-axis coma.

3.2. Off-Axis Astigmatism

Uncorrected, the off-axis astigmatism produced by a paraboloid grows quadratically with distance from the optical axis. This is illustrated in Figure 5, to which some defocus has been added to produce elliptical point spread functions.

Off-axis astigmatism gets rather little attention because relatively few telescopes use a field large enough for it to be appreciable. A notable exception is the paper by McLeod (1995) which describes turning this aberration to benefit by using it to align a wide field telescope. Noethe & Guisard (2000) describe a similar test using the VLT.

We again consider a corrector that has been displaced perpendicular to the optical axis, so that the wrong correction is applied to the astigmatic wavefronts. The mis-corrected images are astigmatic, and the corresponding point spread functions are shown in Figure 6. In the two panels we have added and subtracted some defocus to produce elliptical images. The amplitude of the astigmatism in the miscorrected images grows *linearly* with distance from the center of the field.

The PSF patterns shown in Figure 6 may look daunting, but it takes only three numbers to describe them – the size and direction of the displacement of the correction from the optical axis and the amount of defocus.

The linear growth of the size of the mis-corrected astigmatic images means that the larger the field, the greater the care that must be taken in aligning the telescope. An alignment procedure that works reasonably well for a small field may not work sufficiently well for a larger field. This is in contrast to the case for coma, where the error is the same at all field radii.

3.3. Off-Axis Defocus

In general the focal surfaces of telescopes are curved rather than flat. Such “curvature of field” may be “corrected” either with an optical element or by the use of a curved detector (or small flat detectors approximating a curved surface). A small displacement of the “corrector” perpendicular to the optical axis produces defocus which varies linearly in the direction in which the corrector was displaced. The pattern of aberrations can equivalently be described as a tilt of the focal plane. Two numbers suffice to describe this miscorrection of the curvature of field.

Our use of the term “off-axis defocus” to describe curvature of field is non-standard, but it serves to emphasize that three different circularly symmetric aberration patterns require correction and can be miscorrected. In §5, we will use the term tilt instead, which is more intuitive, especially when considering how the camera can tilt in response to gravity loading.

3.4. Miscellany

Piston errors (i.e. displacements along rather than perpendicular to the optical axis) of the various correction lenses will produce under- or over-corrections and leave a residual off-axis pattern. Piston errors will in general produce a constant defocus. If one piston error is compensated by a second piston error, one produces higher order spherical aberration which varies as ρ^4 in the pupil plane.

Tilt errors of the lenses produce patterns similar to those produced by translations perpendicular to the optical axis.

3.5. Misalignment Summary

A complete description of the point spread functions due to misaligned optics requires seven numbers. Two each for the misalignment of the coma, astigmatism and defocus corrections perpendicular to the optical axis and in finally, the overall defocus of the optical system, which is produced by a displacement of optics (or the detector) *along* the optical axis.

4. Primary Mirror Deformations

The primary mirrors of large telescopes deform as a result of thermal and gravitational stresses. Not all deformations are equally likely. A mirror and its support system have “vibrational” modes whose frequencies increase with mirror stiffness. Static stresses preferentially deform mirrors in those modes that are least stiff. The softest modes are almost always: a) a saddle-shaped deformation that produces wavefront aberrations very much like astigmatism; b) a bowl shaped mode (more nearly conical when the primary has a central hole) that produces wavefront aberrations very much like defocus; and c) a three lobed “trefoil” mode ($\cos 3\theta$ and $\sin 3\theta$) (Noethe 1993).

Large telescopes built after 1990 have “active” optics systems that compensate, in part, for these stresses (Noethe 1993; Schechter et al. 2002). The number of primary mirror modes corrected varies from telescope to telescope. In addition such systems typically correct for translations of the secondary mirror perpendicular to and along the optical axis (which produce, respectively, constant defocus and constant coma). But not all systems are equally active. In some systems only focus is continuously updated in the course of exposures. Coma and astigmatism are measured at longer intervals. Lookup tables are used to correct coma and astigmatism between such measurements.

It is the astigmatism-like and focus-like modes that are of greatest concern for the measurement of weak lensing. A small time-invariant defocus of the telescope will combine with temporal variations in the astigmatism-like mode to produce elliptical PSFs that are roughly constant across the field. Temporal variations in the focus-like mode primary mirror will produce ellipticity if there is any time-invariant astigmatism, perhaps the result of a small telescope misalignment.

Most active optics systems do *not* correct for temporal variations in the focus-like primary mirror mode (but see Schechter et al. 2002). But since this mode produces wavefront aberrations that are nearly degenerate with pistoning of the secondary, most active optics systems correct for this, at least to first order.¹

5. Application to Observed PSFs

Jarvis & Jain (2004) show “whisker” plots showing the shapes of stars observed with the Big Throughput Camera on the Victor Blanco 4-meter telescope (Figure 1 in their paper). They found that the first principal component of the variation seemed to correspond to overall defocus. The plots for images taken very much inside and very outside focus look like uncorrected or partially corrected off-axis astigmatism. Subtracting the best fitting off-axis astigmatism pattern (with focus varying from image to image) a second pattern is evident that has elliptical images oriented diagonally in one corner of one chip and in the perpendicular direction on the opposite chip. One would get such a pattern if, in addition to the off-axis astigmatism one had a time-invariant tilt in the focal plane. This pattern is also evident in the “best focus” frame, for which the off-axis astigmatism would give no ellipticity if the focal plane were not tilted.

These results induced us to try to see whether a physical model of the effects of telescope aberrations might produce a better description of the PSF variation than the purely empirical principal component analysis.

5.1. The Aberration Model

The PSF at any location in the image plane is described by an intensity pattern, $I(x, y)$. We always use sky coordinates, measured in arcsec, for x and y , which means that the effects of telescope distortion are implicitly removed.

We start by defining the shape and size of the PSF as the *unweighted* second moments of the intensity pattern, Q and S :

$$Q(x, y) = \frac{\int dx' dy' I(x', y') z'^2}{\int dx' dy' I(x', y')} \quad (13)$$

$$S(x, y) = \frac{\int dx' dy' I(x', y') |z'|^2}{\int dx' dy' I(x', y')} \quad (14)$$

where $z = x + iy$ gives the location in the image plane, and x' and y' are integrated over the extent of the light distribution for a single PSF (i.e. a single star) centered at z .

The essential causes of the PSF shape and size are the telescope optics and the atmosphere. There are some other minor causes, like diffusion in the CCD, but we neglect these in this model. We assume that the

¹The difference between the focus-like primary mirror mode and piston of the secondary produces spherical-like aberrations.

effects are separable, so Q and S are sums of optics effects and atmospheric effects.

For the optics contribution we can take the photons entering the telescope to be exactly parallel. We also assume that the density of photons is uniform across the pupil. Then the intensity as a function of position in the field, $I(x, y)$ can be obtained by a) subdividing the pupil into (infinitesimal) patches of equal area, b) taking the gradient of the wavefront at each patch, c) taking that gradient to be proportional to the displacement of the light from the nominal image position² and d) summing the contributions to $I(x, y)$ from all patches.

Taking u and v to be the coordinates on the pupil, the PSF at a point in the image plane is given by the pupil plane integrals

$$Q(x, y) = \frac{1}{\int dudv} \int dudv \left(\frac{\partial \delta \lambda}{\partial u} + i \frac{\partial \delta \lambda}{\partial v} \right)^2 \quad (15)$$

$$S(x, y) = \frac{1}{\int dudv} \int dudv \left| \frac{\partial \delta \lambda}{\partial u} + i \frac{\partial \delta \lambda}{\partial v} \right|^2 \quad (16)$$

We insert the wavefront errors due to defocus, astigmatism, coma, and spherical aberration from Equations 2, 5, 6, 9, 10, and 12 and define

$$\begin{aligned} d &= A_{\text{defocus}} \\ a &= (A_{\text{astig-c}} + i A_{\text{astig-s}}) \\ c &= (A_{\text{coma-c}} + i A_{\text{coma-s}}) \\ s &= A_{\text{sph}} \end{aligned} \quad (17)$$

to get

$$Q(x, y) = \frac{1}{\int dudv} \int dudv (2dw + 2aw^* + c(2|w|^2 - 1) + c^*w^2 + 4s|w|^2w)^2 \quad (18)$$

$$S(x, y) = \frac{1}{\int dudv} \int dudv |2dw + 2aw^* + c(2|w|^2 - 1) + c^*w^2 + 4s|w|^2w|^2 \quad (19)$$

where $w = u + iv$ and $*$ denotes complex conjugate. Integrating over the circular pupil, this simplifies to:

$$Q(x, y) = 4 \left(d + \frac{4}{3}s \right) a + \frac{1}{3}c^2 \quad (20)$$

$$S(x, y) = 2 \left(d + \frac{4}{3}s \right)^2 + 2|a|^2 + \frac{2}{3}|c|^2 + \frac{4}{9}s^2 \quad (21)$$

For the defocus value, we include four effects given by four parameters: d_0 is the overall defocus of the camera. d_1 is a tilt of the wavefront as it strikes the camera, which leads to the defocus increasing linearly

² The constant of proportionality is related to the focal length of the telescope. In practice this constant is absorbed into the aberration coefficients, so it is safely neglected.

with field position because the divergence of the rays is proportional to the distance from the center. Thus, the value at any given position is the “dot product” of d_1 with (x, y) . In complex notation this is $\Re(d_1 z^*)$. In addition, we allow for a separate defocus and tilt of each chip in the camera, which we call $d_{0,\text{chip}}$ and $d_{1,\text{chip}}$.

$$d(z) = (d_0 + d_{0,\text{chip}}) + \Re\left((d_1 + d_{1,\text{chip}})\frac{z^*}{R}\right) \quad (22)$$

R is the radius of the field of view, which is included so that d_0 and d_1 have the same units, arc seconds.

The astigmatism value in our model has two components: The primary astigmatism is a_0 , which is constant across the field of view. The miscorrection of the off-axis astigmatism is a_1 . The effect of the a_1 term is derived from taking two copies of the PSF pattern in Figure 5, shifting them and taking the difference. To first order, this is just the derivative. So, since the astigmatism in Figure 5 is proportional to z^2 , the off-axis astigmatism represented by a_1 is proportional to z .

$$a(z) = a_0 + a_1 z \quad (23)$$

Both a_0 and a_1 have units of arc seconds.

As discussed in §3.1, the net effect of coma in the presence of a possibly misaligned corrector lens is a single value, $c(z) = c_0$. Since the misalignment may vary from one exposure to the next, we let c_0 be different for each exposure. There are generally no other significant sources of coma, so this is the only one we include in our model.

We do not expect spherical aberration to vary from one exposure to another, but we do allow for the possibility of some in the telescope design or due to possible slight misplacements of the optical elements. Thus, we could expect there to be a single value of $s(z) = s_0$ for all exposures. However, such a value is completely degenerate with the overall defocus, d_0 , and the atmospheric seeing (discussed below), because only the combination $d + (4/3)s$ appears in the above formulae. Therefore, this combination is taken to be the effective defocus value in the model, and we can thus ignore s entirely.

In addition to the optical model given above, we also add the seeing, S_{atm} to the size. The seeing is not an optical effect of the telescope, but it is obviously the dominant contributor to the PSF size. Therefore, it is absolutely essential to the model. This term also absorbs the $(4/9)s^2$ term that is neglected by ignoring spherical aberration.

The effects of guiding and the average anisotropy of the atmosphere are generally also important. However, since we already have the c_0 term in the formula for Q , these effects are subsumed into that value. There is no way to distinguish coma from guiding errors using only the second moments of the PSF. The trefoil aberration we mentioned above also leads to a constant term in Q (through interactions with the coma), but this is similarly indistinguishable from coma.

We also found it necessary to include an additional function for each of Q and S to describe the base *static* pattern to which the effects of the aberrations for each exposure are added. These functions are called Q_{static} and S_{static} . We use a simple 5th order polynomial for each of these.

So we have the following model for the PSF shape and size as a function of position in the focal plane:

$$Q \approx Q_{\text{model}}(x, y) \equiv 4d(z)a(z) + \frac{1}{3}c_0^2 + Q_{\text{static}}(x, y) \quad (24)$$

$$S \approx S_{\text{model}}(x, y) \equiv 2d(z)^2 + 2|a(z)|^2 + \frac{2}{3}|c_0|^2 + S_{\text{atm}} + S_{\text{static}}(x, y) \quad (25)$$

where $d(z)$ and $a(z)$ are given above in equations 22 and 23.

It is important to note that the terms due to optical aberrations enter the moment equations *quadratically*. As the moment model is linear in Q_{static} and S_{static} , the implication is that these do *not* arise from distortions of the wavefront. This raises the question of just what the source of these static terms might be or if in fact this is the correct functional form to use.

With real data, unweighted moments are not feasible. Instead, we define the shape Q and size S of each observed star with Gaussian weights:

$$Q(x, y) = \frac{\int dx' dy' z'^2 e^{-|z'|^2/2\alpha^2} I(x', y')}{\int dx' dy' e^{-|z'|^2/2\alpha^2} I(x', y')} \quad (26)$$

$$S(x, y) = \frac{\int dx' dy' |z'|^2 e^{-|z'|^2/2\alpha^2} I(x', y')}{\int dx' dy' e^{-|z'|^2/2\alpha^2} I(x', y')} \quad (27)$$

where the scale size, α , of the Gaussian is chosen such that $S = \alpha^2$. (We iterate the choice of α until this is true.) Q and S both have units of arc seconds squared.

Another important consideration is the orientation of the coordinate system we use to define z . The two natural choices are equatorial coordinates, which are oriented east/west and north/south, and alt-az coordinates (also known as “horizon” coordinate), where y is oriented so that it corresponds to the direction of gravity, or up/down, and x is then left/right. Different physical causes for the parameters are more natural in one coordinate system or the other. Anything that is fixed with respect to the orientation of the camera is more natural in equatorial coordinates. Anything that has to do with the gravity loading of the telescope is more natural in alt-az coordinates.

Anticipating that some of the parameters may be connected with gravity loading, we adopt the alt-az choice for z in $d(z)$ and $a(z)$ ³. However, for the static functions $Q_{\text{static}}(x, y)$ and $S_{\text{static}}(x, y)$, we found that it was better to keep x and y in the chip-oriented equatorial coordinates. Similarly, the chip tilts obviously need to be in equatorial coordinates as well, since the direction of the tilt moves with the camera.

There are a few approximations implicit in this model formula, which are worth articulating. First, the formulae for Q and S given in equations 20 and 21 are derived for unweighted moments. However, unweighted moments are impossible on real data, so we use the above Gaussian weight, but this means that the formulae are no longer quite correct.

³ Since the coordinate systems differ only in a phase factor $\exp(i\phi)$, this choice does not affect the χ^2 of the fit, only the covariance matrix and the correlations with hour angle, declination, etc.

Second, the single value for S_{atm} and the incorporation of the anisotropy of the atmosphere into the single value c_0^2 ignore the real variation of the atmospheric component across the field of view. This should not be a significant problem, since the discrepancy for each exposure will be a stochastic function, which will average out over very many exposures (see Jain, Jarvis, & Bernstein 2006 for applications to shear correlation measurements).

Third, we have measured the distortion from the actual positions of stars and galaxies, using overlapping images as well as the USNO astrometric catalog to calculate the overall astrometric solution. However, this solution is constrained to be a 5th order function that is the same for all images plus a simple translation and rotation for each exposure. If the telescope distortion varies from one exposure to the next (for example, from the same kind of decollimations that led to the tilt and off-axis astigmatism) then this will lead to errors.

Fourth, the derivation of equations 20 and 21 assumed uniform illumination across the pupil. This is not actually true. The prime focus camera obscures the center of the pupil. And near the edges of the image, vignetting may be in issue as well.

Finally, there are other higher order aberrations than the ones we have included, which are generally only referred to by their corresponding Zernike polynomial. Similarly, while our expressions for off-axis focus, astigmatism, and coma are correct to first order, there may be terms at higher order in x and y that we have neglected.

5.2. Results

We applied the above methodology for the telescope aberrations to data taken using the Mosaic camera of the Blaco 4-meter telescope at Cerro Tololo Interamerican Observatory (CTIO). The camera has 8 chips, each 2048×4096 pixels with 0.27 arc-second pixels. The field of view has a radius (R in the formulae above) of 18 arcminutes.

We analyzed the PSF shapes from 383 exposures taken in January and July, 2000. For each unsaturated star brighter than 21st magnitude, we measured Q and S and fit them to the above model.

In total, the model has 10 real-valued numbers for each exposure, of which 9 are mis-alignments (d_0, d_1, a_0, a_1, c_0) and the last is seeing (S_{atm}), plus 82 numbers that are constant for all exposures (see Table 1 for the full list of parameters). For 383 exposures, this comes to over 3900 numbers being fit for. To constrain these values, we have almost 400,000 stars, each with three numbers to use, so the model is safely over-constrained.

It would be completely impractical to fit all of these parameters at once, especially since the model is non-linear. So we instead alternate fitting the parameters for each exposure and then the static telescope parameters until the fit converges.

Table 1 lists each of the parameters, along with a summary description and the number of (real) values

Table 1. Parameters used in the PSF Model

Parameter	Description	Number of Real Components	Average Value	Standard Deviation	Marginal Utility	
					χ_Q^2	χ_S^2
<i>Exposure-specific parameters:</i>						
d_0	Primary defocus	1×383	−0.006	0.053	−0.4	3.2
d_1	Off-axis defocus	2×383	0.009 −0.003	0.038 0.040	3.7	4.2
a_0	Primary astigmatism	2×383	0.014 −0.011	0.099 0.089	7.2	−0.5
a_1	Off-axis astigmatism	2×383	0.001 −0.002	0.066 0.055	1.8	0.7
c_0	Coma/guiding shape	2×383	−0.039 −0.010	0.109 0.124	4.7	1.1
S_{atm}	Seeing size	1×383	0.348	0.138	5.7	2.7
<i>Static telescope parameters</i>						
$d_{0,\text{chip}}$	Chip height offsets	7			0.3	1.5
$d_{1,\text{chip}}$	Chip tilts	14			0.4	0.7
Q_{static}	Static shape pattern	40			1.7	0.3
S_{static}	Static size pattern	20			−0.1	2.0

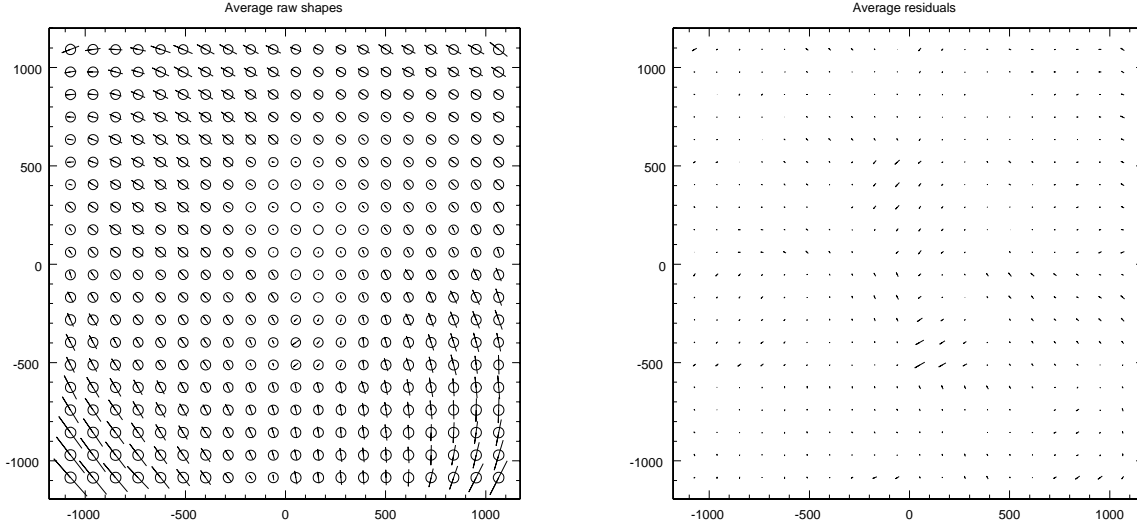


Fig. 7.— The left panel shows the average PSF pattern. The “whisker” lines correspond to the average Q values. The direction indicates the orientation of the ellipse, and the length is proportional to $|Q|$. The circles correspond to the average S values, the size being proportional to the size of the PSF. The right plot shows the difference between the measured and fitted PSF values.

being fit for. It also lists the average values of each of the parameters that change for each exposure, along with their standard deviation. The last column, Marginal Utility, is discussed below in §5.2.

Table 2 gives the normalized covariance matrix for the six exposure-specific parameters. The values are normalized by the standard deviations so the diagonal elements are unity. The matrix is 10×10 , rather than 6×6 , since each complex quantity is treated as two separate real values for this purpose. The table also includes the correlations with hour angle, declination, and zenith distance to indicate which parameters are connected with gravity.

The largest correlation apparent in the data is d_1 with a_1 , both of which also correlate with the direction of gravity, namely the declination and zenith distance.

Figure 7 is a “whisker plot” of the mean PSF pattern averaged over all 383 exposures. The lines (“whiskers”) indicate the shape, Q , at each location. The orientation of the line is the same orientation as the ellipse described by Q , and the length of the line is proportional to $|Q|$. The circles are used to represent the size, S , at each location. The size of the circle is proportional to the value of S .

We can start to see how well the model fits this pattern by plotting the average of the model Q and S values rather than the actual measured values and look at the residual (right panel of Figure 7). The aberration model apparently does manage to describe the data fairly well; however, this is not necessarily a very good test, since we are mostly seeing the static pattern here, which is directly fit using a fifth order polynomial.

A better test is to look at the reduced χ^2 value of the residual PSF anisotropy:

$$\chi_Q^2 = \frac{1}{(N_{\text{star}} - N_{\text{param}})} \sum_i \frac{|Q_i - Q_{\text{model}}|^2}{\sigma_{Q,i}^2} \quad (28)$$

$$\chi_S^2 = \frac{1}{(N_{\text{star}} - N_{\text{param}})} \sum_i \frac{(S_i - S_{\text{model}})^2}{\sigma_{S,i}^2} \quad (29)$$

The total relevant χ^2 value would be $\chi_Q^2 + \chi_S^2$, but we find it instructive to split the quantity into the two parts.

We find the values $\chi_Q^2 = 7.5$ and $\chi_S^2 = 7.0$, compared to initial values of 90.6 and 8014 (i.e. where $Q_{\text{model}} = S_{\text{model}} = 0$). So, we could say that the model is accounting for over 90% of the full description of the PSF shape and over 99% of the description of the size. (The initial size chisq is dominated by the seeing, so the majority of this latter decrease is not an impressive test of the model.)

It is interesting to examine how important each of the parameters used in the model is to the final solution. In particular, we find the marginal utility of each parameter for each of the χ^2 values, which means the amount by which χ^2 increases when each parameter in turn is removed from the model, allowing the other parameter values to adjust to the new model. The primary astigmatism is found to be the most important for the shape, causing an increase of 7.2 when this parameter was removed from the model. (That is, $\chi_Q^2 = 14.7$ in that case.) The marginal utilities of each parameter is listed in Table 1⁴

The only parameter besides the seeing with a significantly non-zero average value is the off-axis astigmatism. This is interesting, since we expect this parameter to be telling us about displacement of optical elements like corrector lenses from the optical axis (see Figure 6). So this may indicate that there is an optical element that is permanently misaligned. However, since the constant offset is in alt-az coordinates, the “permanent” misalignment does move as the telescope changes orientation with respect to the horizon.

6. Discussion

We have presented low order telescope image aberrations as relevant for weak lensing studies with wide field imaging data. We have found that a fairly simple model of the PSF variation, based on an understanding of how focus and astigmatism work and how they can vary across the field, is able to describe approximately 90% of the variation of PSF anisotropy seen in real data. Details of our model and results are given in Sections 5.1 and 5.2.

We find that the astigmatism parameters in our model are moderately correlated with the direction of gravity, suggesting that gravity loading is to some extent responsible for the telescope aberrations.

⁴ Some of these marginal utilities are negative indicating that the fit became slightly better for either Q or S . The maximum likelihood solution minimizes the sum of χ_Q^2 and χ_S^2 , which always increases when a parameter is removed.

At least a portion of the residual PSF is expected to be due to the atmospheric seeing varying across the field of view in each exposure. Newer telescope are expected to have better optical performance; however, even with such improvements, our results suggest that the contribution of telescope optics will remain a significant contributor to PSF anisotropy. This is especially true for surveys that use large numbers of exposures for every field to reduce the atmospheric contribution, since the atmospheric contribution is stochastic in time while the contribution of the telescope optics in consort with gravity loading is not.

Our success in modeling PSF patterns in real data is encouraging for planned surveys that aim to optimize their image quality for weak lensing. On one hand, one can hope to use data taken over the course of the survey to correct telescope misalignments as they occur. On the other, to the extent that such misalignments are not corrected, measurements of the misalignments permit compensation in the data taken using a physical model.

These points have recently been made by Ma et al. (2008), who use ray tracing to map the PSF moments produced by displacements and tilts of the secondary of the space-based SNAP telescope. Their approach differs from the one taken here primarily in that they use detailed models for each of the misaligned elements while we assume that *all* misalignments produce astigmatism, defocus and coma patterns that differ *only* in orientation and magnitude. Secondly, they fit third moments as well as second moments, giving them a better handle on coma and breaking the degeneracy between translations and rotations of their secondary mirror.

More work needs to be done to improve the model and apply it to both understand telescope performance and to gain better precision in PSF interpolation. In §5.1, we listed a number of possible shortcomings of our aberration model. It is unclear to us which of these is the most important to address to make further improvements. We suspect that accounting for the weighted moments may be the most promising direction to proceed.

Another hint is the demarcation of chip boundaries in the residual PSF pattern in Figure 7. Perhaps there is some possible improvement from better modeling of the chips: for example, using a second or third order function for each chip. Also, while we expect that our off-axis astigmatism term is the most important component of astigmatism after the constant primary mirror astigmatism, it is possible that there are other functional forms which are also important to include.

It is worth comparing the efficacy of this model with the purely empirical PCA description of Jarvis & Jain (2004). Since the model uses 10 real numbers for each exposure, we compare it to the PCA model with 5 principal components, each with a complex coefficient. The PCA model leaves a residual $\chi_Q^2 + \chi_S^2$ of $8.5 + 7.0$, compared to the aberration model's $7.5 + 7.0$. So the aberration model is only doing slightly better than the purely empirical method (though a fair comparison is admittedly difficult to formulate). This conclusion may differ for a different telescope or for a larger dataset as expected from upcoming surveys. We leave a more detailed analysis of the performance for follow-up work.

Finally, note that a physical model is unlikely to be able to account for all of the observed PSF pattern. Even aside from atmospheric refraction, the effect of resonance shaking of the telescope, for example, would be exceedingly difficult to model correctly. Jarvis & Jain (2004) found one of their principal components

to correlate with the wind speed in a particular direction. The most likely explanation seems to be that the wind was able to excite a resonance mode in the telescope, which would correspond to an integral of several different misalignment effects coupled in a complicated way. It is hard to imagine that this kind of effect could be effectively included in a physical model like the one we describe here. Therefore, any practical use of this technique would probably have to be followed by a principal component analysis to remove the various more complicated effects that are not included in the model.

We thank Gary Bernstein, Steve Kent and Andy Rasmussen for helpful discussions. This work is supported in part by NSF grant AST-0607667 (at Penn), AST-0602010 (at MIT), the Department of Energy and the Research Corporation.

REFERENCES

- Bernstein, G. M., & Jarvis, M. 2002, *AJ*, 123, 583
- Bowen, I. S., & Vaughn, A. H. 1973, *Appl. Opt.*, 12, 1430
- Hoekstra, H. 2004, *MNRAS*, 347, 1337
- Jarvis M, Jain B. 2004, arXiv:astro-ph/0412234
- Jain B, Jarvis M, Bernstein G. 2006, *JCAP* 2, 1
- Ma Z, Bernstein G, Weinstein A, Sholl M 2008, arXiv:0809.29541
- Mahajan, V. N. 1991, “Aberration Theory Made Simple”, Tutorial Texts in Optical Engineering, Bellingham: SPIE (The International Society for Optical Engineering)
- McLeod, B. 1995, *PASP*, 108, 217
- Noethe, L., 1993, *SPIE*, 1780, 844
- Noethe, L., & Guisard, S. 2000, *A&AS*, 144, 157
- Noethe, L. 2001, arXiv:astro-ph/0111136
- Schechter, P., et al. 2002, arXiv:astro-ph/0207250
- Schneider, P. 2006, *Extragalactic Astronomy and Cosmology*, by Peter Schneider. Berlin: Springer
- Schroeder, D. J. 1999, “Astronomical Optics,” Academic Press

Table 2. Covariance Matrix of Exposure Parameters

	d_0	d_1	a_0	a_1	c_0	S_{atm}
d_0	1	0.15	0.16	0.09	−0.07	0.01
d_1	0.15	1	0.36	0.23	−0.01	0.75
a_0	0.16	0.36	1	−0.04	0.09	0.43
a_1	0.09	0.23	−0.04	1	0.29	−0.11
c_0	−0.07	−0.01	0.09	0.29	1	0.02
S_{atm}	0.01	0.75	0.43	0.20	0.02	1
	0.18	0.29	0.73	−0.11	0.00	0.48
	0.04	−0.15	−0.14	−0.04	0.07	−0.10
	−0.03	0.22	−0.13	0.01	−0.20	0.19
	−0.09	−0.14	0.01	−0.18	0.19	−0.09
HA	−0.03	0.28	−0.06	−0.01	−0.06	0.18
Dec	0.09	0.37	0.39	0.06	0.05	0.27
ZD	0.13	0.20	0.28	0.07	0.03	0.11